Research Article

INTERNATIONAL JOURNAL OF ADVANCED ROBOTIC SYSTEMS

International Journal of Advanced Robotic Systems
September-October 2016: 1–12

DOI: 10.1177/1729881416658167
arx.sagepub.com
SAGE

Modeling of physical human–robot interaction: Admittance controllers applied to intelligent assist devices with large payload

Alexandre Campeau-Lecours[1], Martin J-D Otis[2], and Clément Gosselin[1]

Abstract

Enhancement of human performance using an intelligent assist device is becoming more common. In order to achieve effective augmentation of human capacity, cooperation between human and robot must be safe and very intuitive. Ensuring such collaboration remains a challenge, especially when admittance control is used. This paper addresses the issues of transparency and human perception coming from vibration in admittance control schemes. Simulation results obtained with our suggested improved model using an admittance controller are presented, then four models using transfer functions are discussed in detail and evaluated as a means of simulating physical human–robot interaction using admittance control. The simulation and experimental results are then compared in order to assess the validity and limitations of the proposed models in the case of a four-degree-of-freedom intelligent assist device designed for large payload.

Keywords

Intelligent assist device, human augmentation, large payload, admittance control, human–robot interaction

Date received: 16 February 2016; accepted: 21 May 2016

Topic: Robot Manipulation and Control
Topic Editor: Andrey V Savkin
Associate Editor: Bojan Nemec

Introduction

Human augmentation is an application of robotics in which the force capability of a machine is combined directly with the skill of a human user. The main challenge for human augmentation systems is to perceive the environment and the human intention and then to respond to both adequately and intuitively. Applications involving moderately large payloads often make use of admittance control, in which a handle or a force/torque sensor is used to detect human intention.[1,2]

Although stability issues associated with impedance control have been studied in depth,[3–6] fewer studies have been devoted to admittance control,[7–9,44] or to its modeling.[10] Furthermore, the results presented in these studies are not consistent with observations reported elsewhere[11,12] or with the experimental results obtained in our research. Moreover, in our previous research work,[13] an intelligent assist device (IAD) prototype was characterized and an admittance controller was designed according to the IAD specific characteristics. However, a general physical interactive theoretical model allowing to mathematically demonstrate the stability margin for a general IAD was not developed.

[1] Laval University, Robotics Laboratory, Quebec, Canada
[2] LAIMI Laboratory, Universite du Quebec a Chicoutimi,Chicoutimi, Canada

Corresponding author:
Martin J-D Otis, LAIMI Laboratory, Universite du Quebec a Chicoutimi, Chicoutimi, QC, Canada, G7H 2B1.
Email: martin_otis@uqac.ca

Therefore, this paper presents a new physical interactive model enabling simulations of general IADs. In addition, the proposed model is compared with experimental results on the stability of IADs that use an admittance control scheme. The goal of this work is to evaluate the adequacy of simulations of physical human–robot interaction (pHRI) obtained using the proposed improved models. Such models could also be used for force rendering in haptics, as presented elsewhere,[14,15] or in teleoperation.[16] The underlying challenge in the development of admittance controllers is to increase transparency and thereby improve interaction and reduce mechanical vibrations to below the threshold of human perception.[17]

The following definitions will help the reader to understand the concepts described in this paper.

- Vibration is defined as a transient underdamped response obtained at a constant setpoint and generating exponential decay (real part of the dominant complex pole) of a sinusoidal oscillation (imaginary part of the dominant complex pole pair). When changes in the setpoint are continuous and highly dynamic, a sinusoidal oscillation is observed, usually called a vibration or sometimes ''unstable behavior'' in the literature.
- Transparency refers to the capability of the controller to compensate (feedforward controller) for hardware imperfections such as inertia, friction, backlash and vibration such that the payload and mechanism are hidden while a model (impedance or admittance) is rendered to the user.[18]

Two frequency bandwidths are considered here, in accordance with human perception of vibration (properties of skin mechanoreceptors)[19,17,20] and with human musculoskeletal response (properties of the human body model).[21] It has been found previously that a typical operator is able to control a frequency lower than 10 Hz (i.e. reduce the vibrational amplitude) while higher frequencies are associated with vibrotactile stimulation and can be perceived as a disturbance for a collaborative task.[20,21]

With respect to the state of the art in admittance controller design and technology, the main contribution of this paper is to propose a new model representing physical interaction that can match observations presented in our previous research work[42,13,46] and in others,[11,12] thus allowing humans to operate an IAD more efficiently. The long-term objective is to develop a model of the interaction with industrial IADs in order to understand the effects of each parameter (such as belt stiffness, friction, delay) on the interaction in order to help in designing better cooperative systems. We describe the method used to identify the mechanism physical properties in order to improve the motion controller response and ultimately transparency. The third section presents analysis based on transfer functions and simulations. The simulation results are then compared with the experimental results. Finally, a discussion of the comparison is presented and conclusions are drawn.

Admittance model

Two main types of control are used in haptic applications and pHRI, namely impedance with force feedback and admittance with positional feedback.[22] This article refers to impedance and admittance controllers without reference to the feedback type. Both types of controller may be called ''impedance'' in the literature. Impedance controllers accept a measurement of displacement as input and respond with an adjustment of force. Devices controlled using this method should ideally have low inertia and friction (no hardware imperfections, if possible) since the user will inevitably feel these superfluous forces if compensation for them is inadequate. In contrast, admittance controllers accept a measurement of force as input and respond with a displacement.[12,11,23,24,45] Impedance controllers represent the vast majority of the controllers proposed in the literature and deployed in applications, while admittance controllers are less common since the hardware cost is higher.[25] Their use in pHRI applications has been suggested previously.[26]

Because of the high inertia and friction, it would be too difficult for a human operator to impart movement to the IAD used in this work (shown in Figure 18 and presented in Appendix I), making impedance controllers ill-adapted to the situation, even when a force sensor is used. Prior experience teaches us that the minimal achievable virtual inertia would be about half the real inertia[27] instead of a tenth with admittance control as suggested previously.[11,12] An admittance controller with positional feedback is therefore preferred for both free movement and the constrained motion characterizing our application.

Therefore, we have recently designed a torque-controlled IAD using a feed-forward torque compensation for controlling the actuators aiming at reducing both inertia and friction.[13,42,46] However, those equations did not take into account the dynamic of the physical interaction with the human operator. An initial system model is presented below in order to explain certain aspects to consider when using an admittance controller.

Modeling physical interaction

The one-dimensional admittance equation is written as follows

$$f_H(t) = m(\ddot{x}(t) - \ddot{x}_0(t)) + c(\dot{x}(t) - \dot{x}_0(t)) + k(x(t) - x_0(t)) \quad (1)$$

where $f_H(t)$ is the interaction force (i.e. the force applied by the human operator), m is the virtual mass, c is the virtual damping, k is the virtual stiffness, $x_0(t)$ is the equilibrium point, and $x(t)$, $\dot{x}(t)$, and $\ddot{x}(t)$ are the position, velocity, and acceleration, respectively.

Since simulation of free motion is desired, $k, x_0(t), \dot{x}_0(t)$ and $\ddot{x}_0(t)$ are set to zero. The admittance equation is then rewritten as follows

$$f_H(t) = m\ddot{x}(t) + c\dot{x}(t) \tag{2}$$

The set-point trajectory followed by the end-effector can be described a priori as a position $x_d(t)$ or as a desired velocity $\dot{x}_d(t)$. For velocity control, the desired velocity can be written in the Laplace domain as follows

$$\dot{X}_d(s) = \frac{F_H(s)}{ms + c} = \frac{F_H(s)/c}{\frac{m}{c}s + 1} = F_H(s)H(s) \tag{3}$$

The desired reference in position control then becomes

$$X_d(s) = \frac{F_H(s)}{s(ms + c)} \tag{4}$$

where $X(s)$ refers to the Laplace transform of $x(t)$, $\dot{X}(s)$ is the Laplace transform of $\dot{x}(t)$, $F_H(s)$ is the Laplace transform of $f_h(t)$ and s is the Laplace variable. Velocity control is used here, as chosen previously[28–30] and later explained:[31] with position control, the IAD would be attracted to a given reference position that does not represent the desired human behavior.

Figure 1 presents the control scheme, in which the velocity controller used in the experiments is of the proportional type. Previous experiments showed the effectiveness of proportional gain,[31] thus allowing us to avoid the drawbacks of increased acceleration noise due to the derivative gain and possible decreases in bandwidth due to the integral term (by accumulating error history from human input).

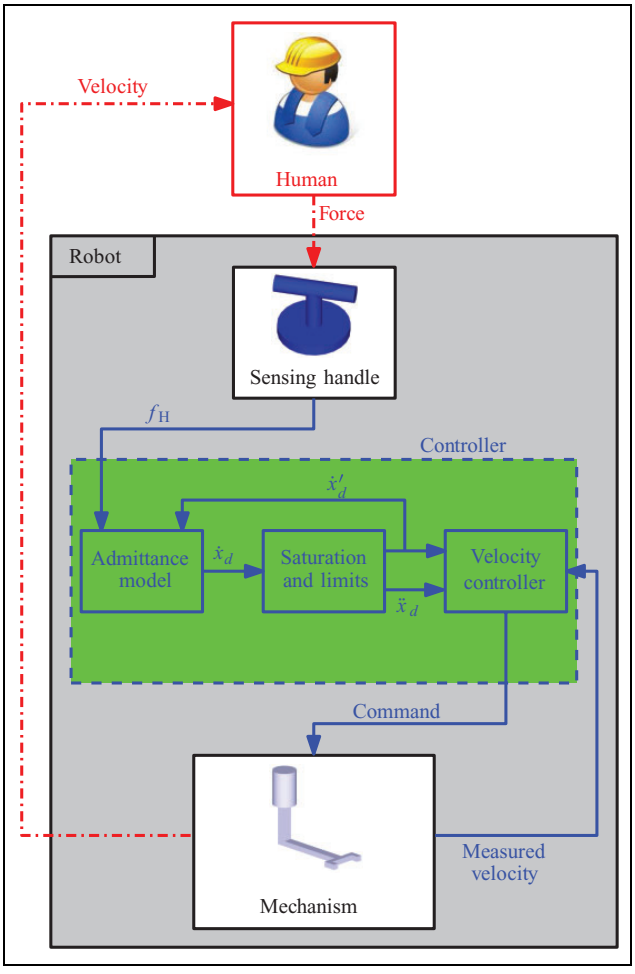

Figure 1. Control scheme used in this work.

Experimental results

The main contribution of this paper is an improved model of interaction in a closed loop. Results found in the literature are not consistent and suggested where controller design could be improved. A device described previously in Appendix I was used with an admittance controller. This set-up provided clear experimental proof that there is a lower boundary on the virtual mass that the system can stably render, which is consistent with results presented previously.[11,12] Below this mass, vibrations or instability may occur when the operator is stiff (a stiff environment is known to favor system vibrations or instability[27]). We also obtained experimental proof that a high virtual mass can be rendered even when the operator is stiff.

The minimal virtual mass that can be rendered for different values of virtual damping was determined experimentally for the X and Y axes of the IAD. These masses are shown in Figure 2. In the vibration-free zone, human perception of vibration is negligible for any operator motion, even under conditions of stiffness.[17] The line separating the zones was obtained by lowering the virtual mass until the operator sensed a vibration that made the interaction uncomfortable. This test involved quickly varying interaction forces and/or stiff operator movements. When determining the minimal mass, one should ensure that the velocity controller is not the cause of device vibrations. It is apparent on the graphs that a critical damping exists (60 Ns/m for the IAD used here) below which it becomes difficult to render fast dynamics. Moreover, the ratio of minimal virtual mass to virtual damping seems to converge to a limit value as damping increases. Stability constraints are more stringent for motion along the X axis than along the Y axis, due to greater inertia and compliance along the X axis in the device used here.

The experimental results show that in a stiff environment with a given damping, a minimal virtual mass exists for which the IAD is vibration-free (sometimes termed stable in the literature). Our experiment led to the observations summarized below.

- There is no evidence for a maximal mass leading to vibration and then instability. This result is in accordance with statements made in previous reports without experimental validation or detailed explanation using a physical model,[11,12] and in contrast with conclusions reached elsewhere that there is no evidence

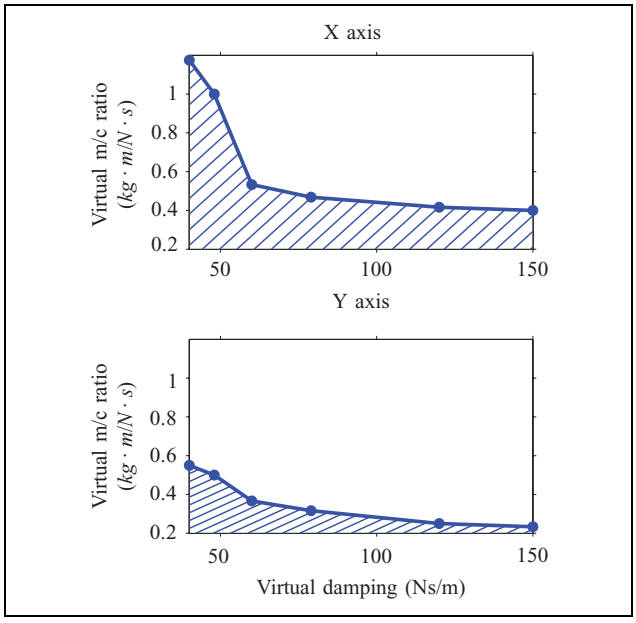

Figure 2. Stability limits for motion along the *X* and *Y* axes: ratio of minimal virtual mass to virtual damping versus virtual damping. The area below the plotted line corresponds to vibrations that can be felt by the operator, while the area above is the vibration-free zone.

for the existence of a minimal virtual mass while a maximal authorized mass might exist.[7–9]

- All authors agree that increasing virtual damping decreases system transparency but improves the perception of vibration or reduces distraction due to mechanical vibration.
- Experimental results show that it is counterintuitive to cooperate under conditions of high virtual-mass-to-damping ratio, since movement of the payload is difficult to stop or decelerate once started.

These observations are sufficient to justify the study of an improved physical model. The development of this model from open to closed-loop feedback is presented below.

Towards the development of an effective model

The mathematical models used to analyze the regions of cooperation, vibration and instability as identified experimentally and described in the preceding section are presented below. The proposed analysis is based on the Laplace plane, the Routh–Hurwitz stability criterion and simulations suggested previously.[32]

The first model considers an ideal case: both the controller and the mechanism are transparent. In other words, the admittance causality is able to hide the mechanism suitably from human perception. A transfer function called *imperfections*[33] is also added to represent different issues

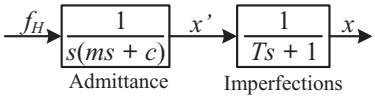

Figure 3. Simple open-loop model.

such as signal filtering (reducing the bandwidth), imperfect control (controller gains are not accurate) and small delays. Using these assumptions, models with the human operator in open-loop and closed-loop feedback are analyzed.

The open-loop model

In this model, it is assumed that the operator simply applies interaction forces as represented in Figure 3 where s is the Laplace variable, m is the virtual mass, c is the virtual damping, $f_H(t)$ is the interaction force (i.e. the force applied by the operator), $x(t)$ is the position, $x'(t)$ is an intermediate result, and T is a time constant related to parameters modeling bias and imperfection.

The transfer function can be written as follows:

$$\frac{V(s)}{F_H(s)} = \frac{1/c}{(\frac{m}{c}s+1)(Ts+1)} \tag{5}$$

where $V(s)$ is the Laplace transform of the velocity $v(t)$ (time derivative of $x(t)$) and $F_H(s)$ is the Laplace transform of $f_H(t)$.

For a given input, the steady-state velocity is lower for a higher virtual damping. The virtual mass has a low-pass effect, thereby filtering force sensor noise and high variation of the interaction force (when the operator applies physical effort to the end-effector). However, if the virtual mass is too high, cooperation becomes counterintuitive since acceleration takes time and once in progress, is difficult to oppose.

The simplified closed-loop model

The second model assumes that the operator acts as a spring system that tends to remain at a given position, thus simulating stiffness, as represented in Figure 4 where K_H is the human operator stiffness and $x_{hd}(t)$ is the desired operator position (set at zero in the simulations). The human arm model is based on a previous study where an estimation of human arm stiffness was performed in a human–robot cooperative calligraphy task.[28]

The transfer function can be written as follows:

$$\frac{V(s)}{F_H(s)} = \frac{s}{mTs^3 + (cT+m)s^2 + cs + K_H} \tag{6}$$

We shall now analyze the stability of the closed-loop transfer function using the position of its pole in the s-plane (complex plane on which Laplace transforms are graphed) along with the Routh–Hurwitz stability criterion. Applying

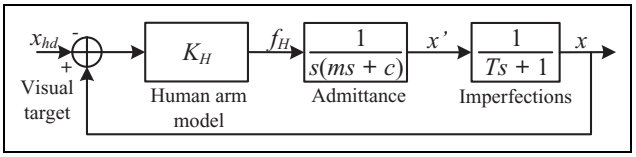

Figure 4. Simple closed-loop model.

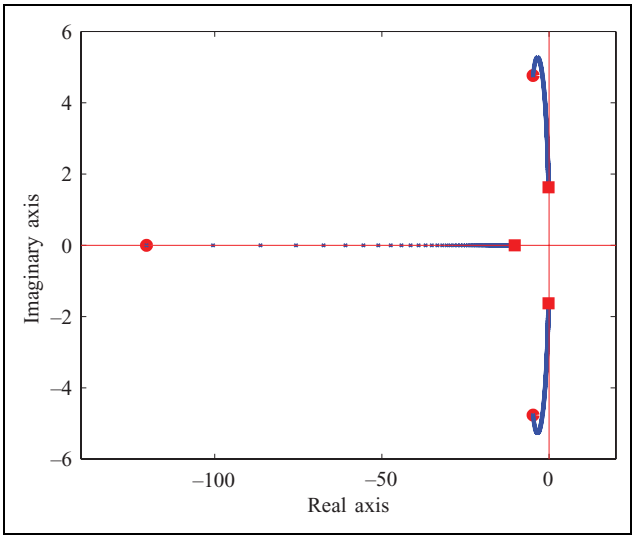

Figure 5. Poles of the simple closed-loop model for case (2) ($c - TK_H > 0$) for a virtual mass varying from 1 kg (circle) to 200 kg (square), $c = 120$ Ns/m, $T = 0.1$ s and $K_H = 550$ N/m.

the Routh–Hurwitz criterion to equation (6), the condition under which the system is stable is defined as follows:

$$c^2T + cm - mTK_H = m(c - TK_H) + c^2T > 0 \quad (7)$$

For a given damping, imperfection and stiffness, equation (7) yields three cases, namely: (a) $c - TK_H = 0$; (b) $c - TK_H > 0$; and (c) $c - TK_H < 0$. For the first two cases, it is readily observed that the poles are located on the left-hand side of the Laplace plane for any value of the virtual mass. In the third case, the system will be stable when the virtual mass meets the following condition:

$$m < \frac{c^2T}{TK_H - c} \quad (8)$$

For example, for the realistic values $c = 20$ Ns/m, $T = 0.1$ s, $K_H = 550$ N/m, $m < 1.14$ kg is obtained.

For case (b), obtained from a well-designed virtual damping, we learn that a greater mass leads to a more underdamped system, without crossing to the right-hand side of the Laplace plane, as shown in Figure 5. The pole starting points are each represented by a dot and the parameter variation is directed toward a square. It should be pointed out that these graphs show the evolution of the poles with regard to a varying parameter and therefore do not represent a classical root locus. The evolution of the poles is very similar to what would be obtained with a

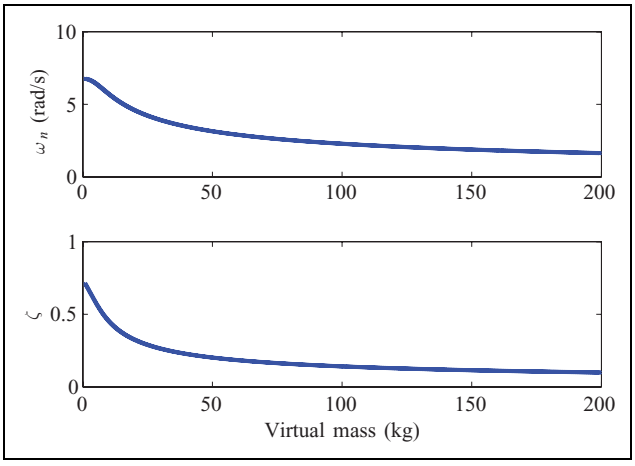

Figure 6. Natural frequency and damping ratio for underdamped poles as a function of virtual mass varying from 1 to 200 kg, $c = 120$ Ns/m, $T = 0.1$ s and $K_H = 550$ N/m.

simple mass–damper–spring system. This analysis gives a maximal mass with which it is intuitive to collaborate for a given damping, since once the mass is in motion it is difficult to stop. In practice, the oscillations so induced are of very low frequency and the operator would be able to control the system.

Based on this model, the following observations can be made:

- if the virtual mass increases, the natural frequency and damping ratio decrease and stabilize asymptotically as shown in Figure 6;
- for a low virtual mass, the system is more damped but the frequencies are higher;
- even if the system is more damped for low virtual masses, the result is worse since the vibrations occur at higher frequencies; these oscillations make control of the device more difficult and uncomfortable since they are in the skin mechanoreceptor sensitivity range;[34]
- with higher virtual mass, the damping ratio is lower but the low frequency of the vibration makes it manageable for the human operator;
- higher virtual mass reduces the impact of the force sensor noise.

For case (c) where $c - TK_H < 0$, the poles are shown in Figure 7 for different values of m. Both poles are located on the right-hand side of the Laplace plane, except for virtual masses below a given value. For the given example, the maximal mass is 13 kg. Our virtual mass would have to be less than this for the poles to be located on the left-hand side of the Laplace plane (i.e. for the system to be stable). This analysis has been used previously[8] for the online computation of the critical mass or damping that ensures stability. The goal pursued in the latter study was to ensure stability in the case of $c - TK_H < 0$. However, since others

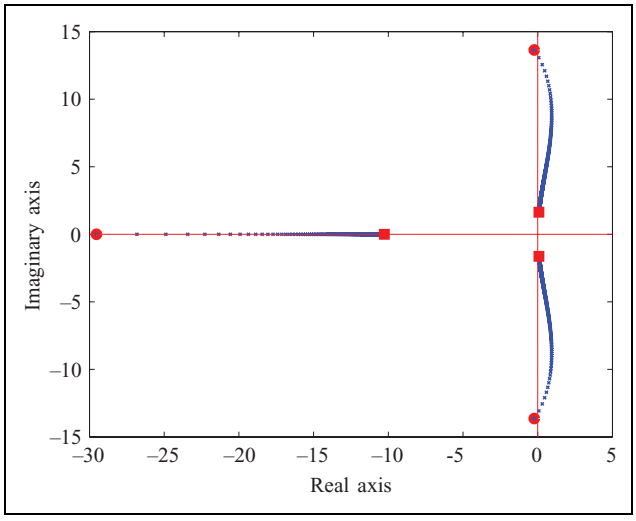

Figure 7. Poles for a simple closed-loop model for case (2) for a virtual mass varying from 1 kg (circle) to 200 kg (square), $c =$ 20 Ns/m, $T = 0.1$ s and $K_H = 550$ N/m.

found that the minimal achievable virtual mass was six to ten times lower than the real mass,[11,12] which was confirmed experimentally in the present work, it seems that it would be very difficult to render the low virtual masses thus computed. For instance, as detailed in Appendix I, the mass of the IAD used in this work is 500 kg, suggesting a minimal virtual mass of 50 kg,[11,12] far more than the maximal virtual mass target of 13 kg found here. In other words, it would be very difficult for the controller to render such a small virtual mass. Our experience shows that trying to do so results in large vibrations. Even assuming that it might be possible to render such a virtual mass with a high-performance IAD, the poles shown in Figure 7 correspond to high frequencies and are very underdamped. The operator would very likely perceive such vibrations and cooperation would be counterintuitive and uncomfortable.

Based on this analysis, we can conclude the following:

- although a theoretical stable zone exists for case (c), it is not practical since it may not be reachable and if it were, it would lead to a very underdamped response;
- it is therefore preferable to modify the virtual damping and mass in order to satisfy case (b) with a damped response perception, since the cooperation must not only be stable but also intuitive and free of vibration;
- the model presented in this section indicates that there is a minimal virtual damping below which the system is unstable;
- the model cannot predict the existence of a minimal mass, as obtained in the experiments and reported in the literature.[11,12]

Although this simple model may be used as a guideline, it does not suitably represent reality. An improved model was therefore developed, as described below.

Proposed improved closed-loop model

A more elaborate model of the IAD developed in order to alleviate the drawbacks of the simple model presented above is illustrated schematically in Figure 8, where m_R represents the motor inertia, C_B represents the mechanical transmission damping, K_B represents stiffness, C_R is the viscous friction acting on moving mass M_R, and F is the actuation force. In the IAD used in this work, circular toothed belts transmit the power from the actuators to the end-effector. Therefore, C_B and K_B represent belt damping and stiffness.

Open-loop version

The open-loop model is represented in Figure 9, where K_P is the control gain.

The human force input is transformed into a velocity through the admittance law stated previously in (3). The velocity error is then filtered, sent to a controller (proportional gain acting as a follower) and the resulting command $F(s)$ is sent to the IAD actuators. This model allows the inclusion of compliance, control imperfection and delay. The corresponding transfer function is given in equation (9) developed in Appendix II. The location of the poles, as a function of the virtual mass, is shown in Figure 10. It should be noted that the ratio of virtual mass to damping corresponds to the real pole (which varies with the virtual mass) while the others remain constant.

In this case, the effect of the virtual mass is quite simple: as it increases, so does its filtering effect, and the desired velocity is accordingly smoother. Figure 11 shows the time response to an operator step force input for low and high virtual mass. A high virtual mass helps to decrease the amplitude of the vibrational envelope. If the virtual mass is low, the response may be underdamped when the interaction force varies abruptly. This is in accordance with the experiments, in which a low virtual mass led to vibration.

Figure 14 compares the simulations and experimental results. The open-loop curve was obtained by simulating different virtual masses for a given virtual damping. The minimal mass was selected when the velocity difference between a maximum and minimum was equal to 0.15 m/s for a force of 100 N applied for 3 seconds. These values were selected heuristically and from experimental results.

The open-loop model provides partial explanation of the vibration problem (human perception of an underdamped response) including transmission compliance, time delay and control imperfection in the case of low virtual mass.

Improved closed-loop version

The open-loop model presented in the preceding subsection leads to results that are consistent with experiments in the sense that it predicts the existence of a minimal mass. However, it does not explain the minimal mass effect for

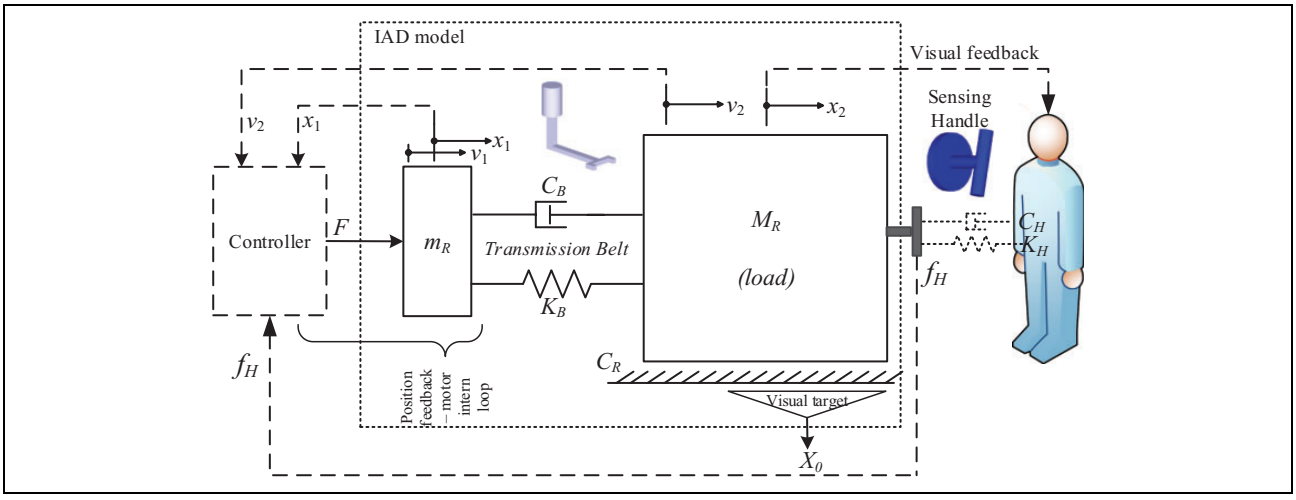

Figure 8. Improved IAD model.

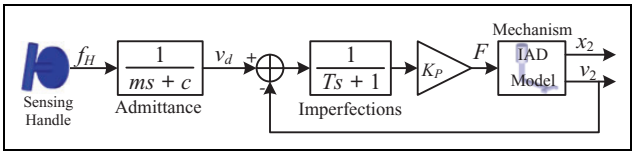

Figure 9. Improved open-loop model.

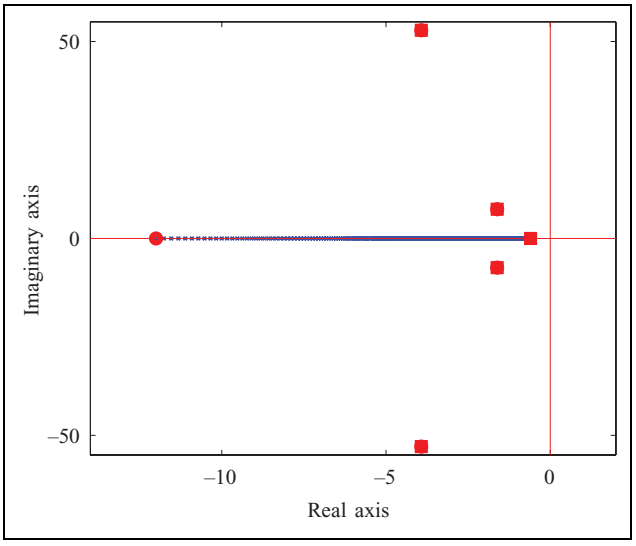

Figure 10. Poles of the improved open-loop model for a virtual mass varying from 10 kg (circle) to 200 kg (square), $c = 20$ Ns/m, $T = 0.1$ s, $Kp = 10,000$, $M_R = 500$ kg, $C_R = 100$ Ns/m, $m_R = 50$ kg, $K_B = 40,000$ N/m, $C_B = 40$ Ns/m.

low damping. A detailed model with the human operator in a closed loop was therefore studied.

The improved model requires a human arm dynamic model in the closed-loop control system. A detailed model including the vestibular system, reflex mechanisms and other motor functions has been presented previously.[35,36] Three-dimensional arm modeling in space could also be

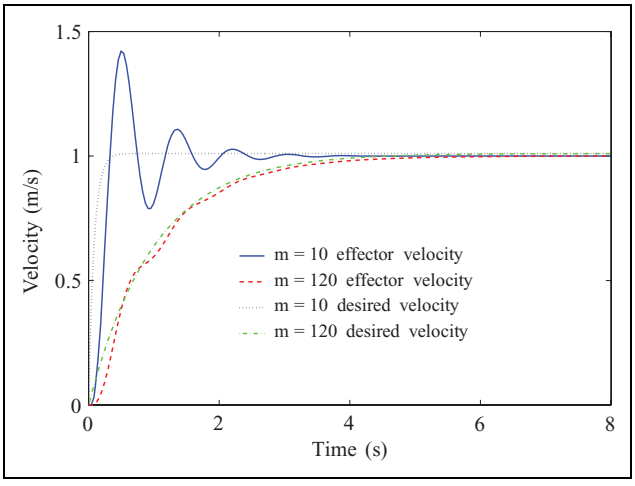

Figure 11. Human force step response: $c = 20$ Ns/m, $T = 0.1$ s, $Kp = 10,000$, $M_R = 500$ kg, $C_R = 100$ Ns/m, $m_R = 50$ kg, $K_B = 40,000$ N/m, $C_B = 40$ Ns/m.

used.[37] However, we need an end-point impedance model applied in collaborative work with a robot.[38] Also, since another study suggests that visual perturbation does not influence stiffness control,[39] the visual delay was removed. Finally, since the dynamic model is represented in one degree-of-freedom (1 DOF), a damping parameter C_H was added over the previous simple model presented in Figure 4 as other works suggest.[28] Our human arm model is then represented schematically in Figure 12. The corresponding transfer function is given in equation (11) in Appendix I. Pole location is shown in Figure 13 for a varying virtual mass.

An underdamped response and an unstable zone occur below a given virtual mass, as observed in the experiments. Figure 14 compares the stability or vibrational limits obtained in simulations and experiments. For a perturbation of the force of 1 N for 0.05 s, the minimal mass was obtained when the oscillations reached an amplitude of

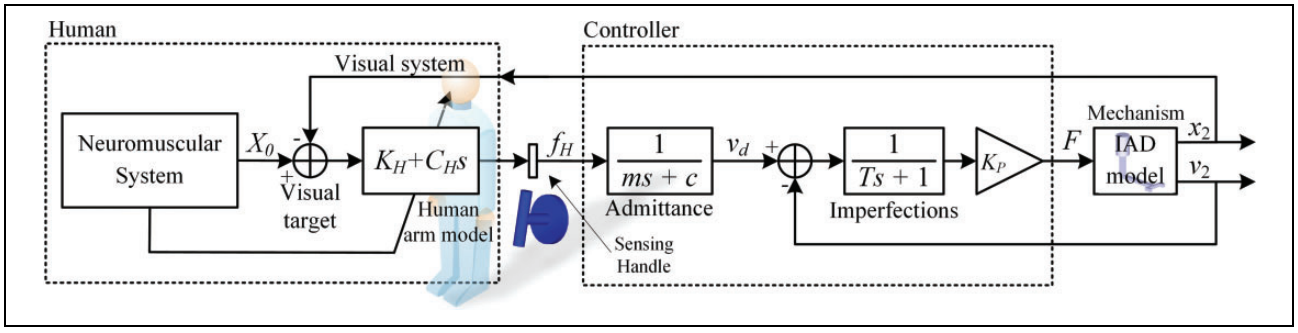

Figure 12. Improved closed-loop model.

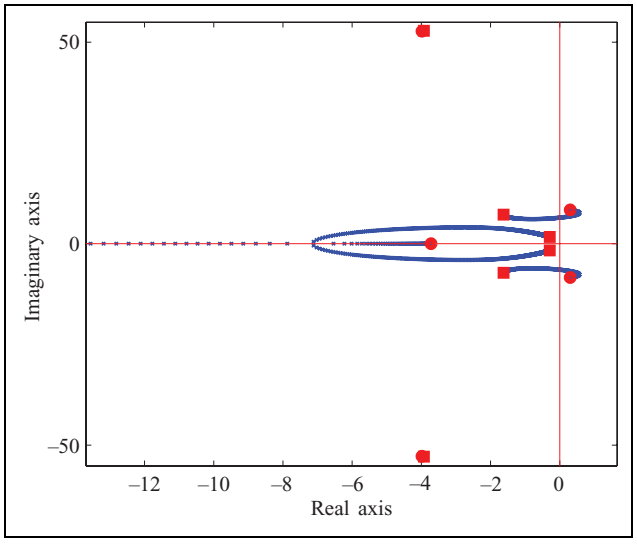

Figure 13. Location of the poles of the improved closed-loop model for a virtual mass varying from 0.1 kg (circle) to 200 kg (square), $c = 20$ Ns/m, $T = 0.1$ s, $Kp = 10,000$, $M_R = 500$ kg, $C_R = 100$ Ns/m, $m_R = 50$ kg, $K_B = 40,000$ N/m, $C_B = 40$ Ns/m, $K_H = 550$ N/m, $C_H = 23.45$ Ns/m.

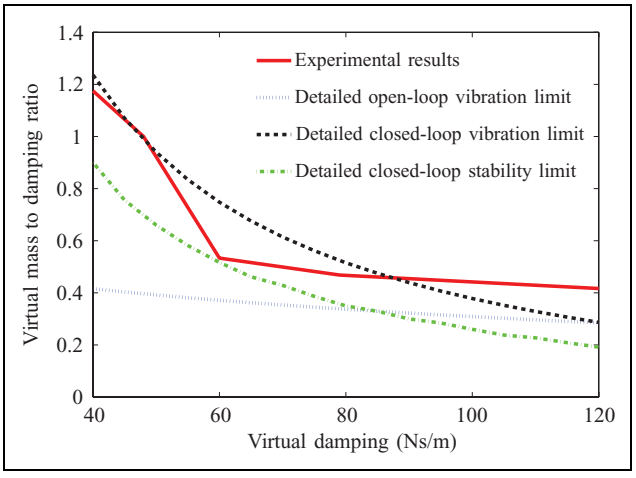

Figure 14. Comparison of the ratio of minimal stable/acceptable virtual mass to virtual damping obtained using simulation models and experimental data.

0.013 m/s. These values were selected heuristically and from experimental results. The minimal stable mass was obtained by lowering the virtual mass in the simulation until the system became unstable.

The results are very similar to experimental observations:

- the model satisfactorily predicts the existence of a minimal virtual mass and characterizes the variation thereof with respect to virtual damping;
- no maximal virtual mass leading to instability was found, which is consistent with the experimental results obtained here and previously[11,12] (however opposite conclusions have been reached elsewhere,[7–9] as explained above);
- for very high virtual masses, interaction is not intuitive since the motion is very underdamped and difficult to stop once started.

It would be possible (though more difficult and not intuitive) for the operator to compensate for such motion, since these phenomena occur at very low frequency. It has been found experimentally[11,12] and confirmed with the present model that the minimal virtual mass has a much greater impact than does the maximal intuitive virtual mass. The main reason for this is that the virtual mass must be minimized in order to reduce the required force input from the operator. The minimal mass is therefore obviously the primary concern.

Transmission stiffness

Figure 15 shows the poles of the improved open-loop model for varying transmission stiffness. It is apparent that stiffer transmission leads to better results while compliant transmission may lead to vibration as shown in Figure 16. However, a somewhat compliant end-effector may be beneficial since it does not affect transmission stiffness but limits the "stiffness" of the environment.

Discussion

The existence of a minimal virtual mass that eliminates perceptible vibration was observed experimentally and was

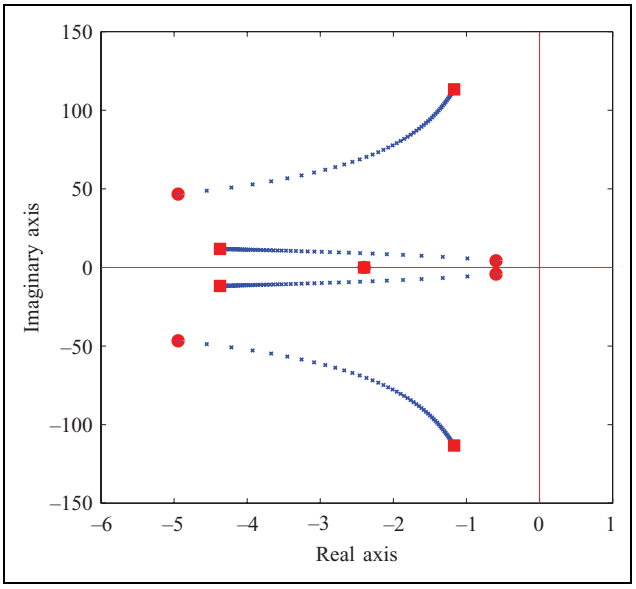

Figure 15. Location of the poles of the improved open-loop model for transmission stiffness varying from 10,000 N/m (circle) to 500,000 N/m (square), $c = 20$ Ns/m, $T = 0.1$ s, $Kp = 10,000$, $M_R = 500$ kg, $C_R = 100$ Ns/m, $m_R = 50$ kg, $K_B = 40,000$ N/m, $C_B = 40$ Ns/m.

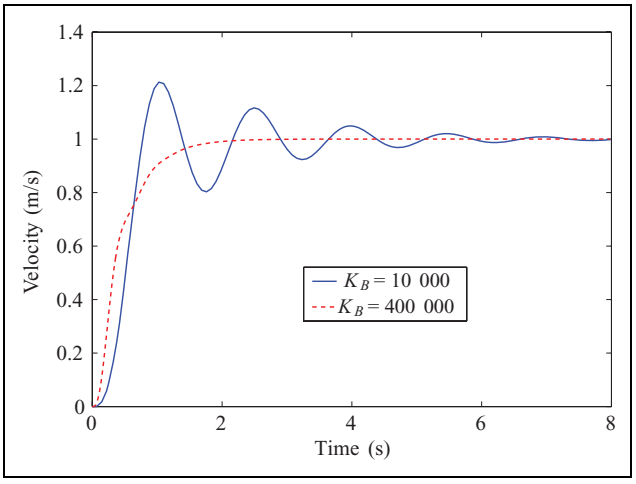

Figure 16. Human force step response for the improved open-loop model for low and high transmission stiffness ($c = 20$ Ns/m, $T = 0.1$ s, $Kp = 10,000$, $M_R = 500$ kg, $C_R = 100$ Ns/m, $m_R = 50$ kg, $C_B = 40$ Ns/m).

explained using the improved model. It was found that the system may vibrate even in an open-loop configuration if the virtual mass is low and the force profile is highly dynamic. This result is related to the velocity controller and to the mechanism bandwidth. The virtual mass should be high enough so that the system does not oscillate with an open-loop controller, since otherwise the admittance equation will not be well rendered, thus reducing transparency.

It was also found that in a stiff environment (i.e. in a closed loop), the system may oscillate and even become unstable if the virtual mass is too low. It is clear that if the

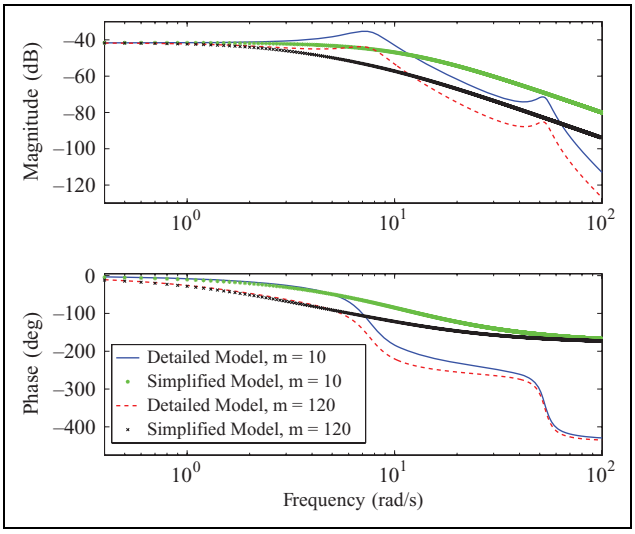

Figure 17. Bode plot in an open-loop control configuration: $c = 20$, $T = 0.1$, $Kp = 10,000$, $M_R = 500$, $C_R = 100$, $m_R = 50$, $K_B = 40,000$, $C_B = 40$.

mass is low enough for the system to oscillate when the controller is in an open-loop configuration, it is very likely to oscillate with a closed-loop controller. The virtual mass must be high enough so that the operator will be comfortable in both control modes. The notion of comfort is associated with the perception of vibrations, which are related to the oscillation frequency and amplitude. High-frequency vibrations are less comfortable since they are impossible for the operator to manage, due to physical[21] or cognitive limitations. The control system, virtual damping and mechanism must be well designed in order to allow ergonomic and vibration-free interaction. It should also be noted that the human perception bandwidth varies significantly between the fingertips and the larger muscle groups.[21,40,41] The required operator forces should therefore remain low. Although it is possible to manage low-frequency oscillations that occur when the virtual mass is large, interaction may be less intuitive in such cases, as explained previously.

Figure 17 presents the Bode plot of the open-loop models (simple and improved) for two virtual masses. For the improved model, the cut-off frequency is 0.16 Hz at $m = 120$ kg and 1.3 Hz at $m = 10$. In addition, the 6.4 dB peak observed at $m = 10$ can lead to overshooting and vibration. As shown on Figure 17, the simple model is never unstable as we never reach a phase passing through $-\pi/2$ rad and 0 dB gain. However, this does not have any consequence on perceptible vibrations as in higher frequency on the Bode plot, the system can oscillate in transient response. Then, an operator can stimulate this response by applying an opposite force on the handle which generates continuous oscillation until the arm stiffness is reduced. When using the improved model, the system could be unstable with a 42 dB ($m = 10$ kg, $w_g = 9.7$ rad/s) and 52 dB ($m = 120$ kg, $w_g = 7.8$ rad/s) gain margin in open loop. This model suggests a reduction of the

gain margin while reducing virtual mass until a critical mass where the system is unstable. The improved model is then a better assumption than the simple one when instability (exponentially increasing vibration) should be avoided in the robot control design.

Conclusion

In order to achieve effective augmentation of human capacity using motorized mechanical devices, cooperation with the device must be very intuitive and safe for the operator. In this study, safety was related to vibrational disturbance, which could decrease the attention given to a task and thus lead to injury if the task were limited in time and involved risk. We have presented an analysis of the stability and intuitiveness of an assistive device using an admittance control scheme. The focus of our analysis was evaluation of models simulating pHRI. Four such models were developed and presented in detail, while experimental results provided insight into the ability of each model to simulate the interaction paradigm. The simple model found in the literature yielded functional results but was unable to reproduce suitable behaviors in response to certain situations encountered in practice, namely high-frequency underdamped response (vibration) when the virtual mass is low. A more elaborate open-loop model explained in part the behavior encountered in practice, namely the existence of a minimal virtual mass, but not its variation with virtual damping. Finally, based on our experience and experimental setups, we developed a more elaborate and improved closed-loop model. This model gave results very close to those obtained in our experiments and explained both the minimal virtual mass and its variation with virtual damping. This model leads to better comprehension of the mechanism under study.

In future work, we will use this model in simulations in order to design better systems. A design method for selecting the values of the virtual parameters will be proposed as well. This method will be based on a performance and perception study for evaluating the capability of human operators to manage an IAD for different tasks and in different situations as well as threshold amplitudes at which vibration with disturbance is perceived (visually and audibly).

Declaration of conflicting interests

The author(s) declared no potential conflicts of interest with respect to the research, authorship, and/or publication of this article.

Funding

The author(s) disclosed receipt of the following financial support for the research, authorship, and/or publication of this article: This work was supported by the Natural Sciences and Engineering Research Council of Canada (NSERC) (grant number DG 89715).

References

1. Kosuge K and Kazamura N. Control of a robot handling an object in cooperation with a human. In: *6th IEEE International Workshop RO-MAN Proceedings*, 1997, pp. 142–147.
2. Colgate JE, Peshkin M and Klostermeyer SH. Intelligent assist devices in industrial applications: a review. In: *Proceedings of the International Conference on Intelligent Robots and Systems*, 2003, pp. 2516–2521.
3. Jung S and Hsia T. Stability and convergence analysis of robust adaptive force tracking impedance control of robot manipulators. In: *IEEE International Conference on Intelligent Robots and Systems*, 1999, vol. 2, pp. 635–640.
4. Zeng G and Hemami A. An overview of robot force control. *Robotica* 1997; 15: 473–482.
5. Surdilovic D. Robust control design of impedance control for industrial robots. In: *IEEE International Conference on Intelligent Robots and Systems*, 2007, pp. 3572–3579.
6. Chien MC and Huang AC. Adaptive impedance control of robot manipulators based on function approximation technique. *Robotica* 2004; 22: 395–403.
7. Tsumugiwa T, Yokogawa R and Yoshida K. Stability analysis for impedance control of robot for human–robot cooperative task system. In: *Proceedings of the IEEE/RSJ International Conference on Intelligent Robots and Systems*, vol. 4, 2004, pp. 3883–3888. DOI: 10.1109/IROS.2004.1390020.
8. Duchaine V and Gosselin C. Investigation of human–robot interaction stability using Lyapunov theory. In: *IEEE International Conference on Robotics and Automation*, 2008, pp. 2189–2194. DOI: 10.1109/ROBOT.2008.4543531.
9. Duchaine V and Gosselin C. Safe, stable and intuitive control for physical human–robot interaction. In: *IEEE International Conference on Robotics and Automation*, 2009, pp. 3383–3388.
10. An CH and Hollerbach J. Dynamic stability issues in force control of manipulators. In: *American Control Conference*, 1987, pp. 821–827.
11. van der Linde R and Lammertse P. HapticMaster - a generic force controlled robot for human interaction. *Industrial Robot: An International Journal* 2003; 30: 515–524.
12. Lammertse P. Admittance control and impedance control - a dual, 2004. Available at: http://www.haptist.com/resources/Lammertse_2004_admittance_impedance_control_dual.pdf (accessed 15 March 2011).
13. Lecours A and Gosselin C. Computed-torque control of a four-degree-of-freedom admittance controlled intelligent assist device: *International Symposium on Experimental Robotics* (Springer Tracts in Advanced Robotics). New York: Springer, 2013, pp. 635–649.
14. Ott C, Mukherjee R and Nakamura Y. A hybrid system framework for unified impedance and admittance control. *Journal of Intelligent and Robotic Systems* 2015; 78: 359–375.
15. Otis M, Duchaine V, Billette G, Perreault S, Laurendeau D and Gosselin C. Cartesian control of a cable-driven haptic mechanism. In: Otis MJ-D, et al. (eds) *Advances in Haptics*. InTech, 2010, pp. 75–102

16. Daniel R and McAree R. Fundamental limits of performance for force reflecting teleoperation. *The International Journal of Robotics Research* 1998; 17: 811–830.
17. Jones LA and Sarter NB. Tactile displays: Guidance for their design and application. *Human Factors: The Journal of the Human Factors and Ergonomics Society* 2008; 50: 90–111.
18. MacLean KE. Foundations of transparency in tactile information design. *IEEE Transactions on Haptics* 2008; 1: 84–95.
19. Visell Y. Tactile sensory substitution: Models for enaction in HCI. *Interacting with Computers* 2009; 21: 38–53.
20. Dargahi J and Najarian S. Human tactile perception as a standard for artificial tactile sensing - a review. *The International Journal of Medical Robotics and Computer Assisted Surgery* 2004; 1: 23–35.
21. Jarrah M, Wassem W, Othman M and Gdeisat M. Human body model response to mechanical impulse. *Medical Engineering and Physics* 1997; 19: 308–316.
22. Carignan C and Cleary K. Closed-loop force control for haptic simulation of virtual environments. *Haptics-e* 2000; 1(2): 1–14.
23. Hayward V and Maclean K. Do it yourself haptics: part I. *IEEE Robotics Automation Magazine* 2007; 14(4): 88–104.
24. Lammertse P, Frederiksen E and Ruiter B. The HapticMaster, a new high-performance haptic interface: *Proceedings of Eurohaptics*, Edinburgh, UK, July 2002, pp. 1–5.
25. Faulring E, Lynch K, Colgate J and Peshkin M. Haptic display of constrained dynamic systems via admittance displays. *IEEE Transactions on Robotics* 2007; 23: 101–111.
26. Lee S, Hara S and Yamada Y. A safety measure for control mode switching of skill-assist for effective automotive manufacturing. *IEEE Transactions on Automation Science and Engineering* 2010; 7: 817–825.
27. Colgate E and Hogan N. An analysis of contact instability in terms of passive physical equivalents. In: *Proceedings of the IEEE International Conference on Robotics and Automation*, 1989, vol. 1, pp. 404–409.
28. Tsumugiwa T, Yokogawa R and Hara K. Variable impedance control based on estimation of human arm stiffness for human–robot cooperative calligraphic task. In: *Proceedings of the IEEE International Conference on Robotics and Automation*, 2002, vol. 1, pp. 644–650.
29. Ikeura R and Inooka H. Variable impedance control of a robot for cooperation with a human. In: *Proceedings of the IEEE International Conference on Robotics and Automation*, 1995, vol. 3, pp. 3097–3102.
30. Tsumugiwa T, Yokogawa R and Hara K. Variable impedance control with regard to working process for man–machine cooperation-work system. In: *Proceedings of the IEEE/RSJ International Conference on Intelligent Robots and Systems*, 2001, vol. 3, pp. 1564–1569.
31. Lecours A, Mayer-St-Onge B and Gosselin C. Variable admittance control of a four-degree-of-freedom intelligent assist device: *Proceedings of the IEEE International Conference on Robotics and Automation (ICRA)*, Saint Paul, MN, 2012, pp. 3903–3908.
32. Gil J, Avello A, Rubio A and Florez J. Stability analysis of a 1 dof haptic interface using the Routh–Hurwitz criterion. *IEEE Transactions on Control Systems Technology* 2004; 12: 583–588.
33. Lee T and Tsay S. Approximate solutions for linear time-delay systems via pade approximation and orthogonal polynomials expansions. *Control, Theory and Advanced Technology* 1987; 3: 111–128.
34. Vallbo A and Johansson R. Properties of cutaneous mechanoreceptors in the human hand related to touch sensation. *Human Neurobiology* 1984; 3: 3–14.
35. Burdet E, Tee KP, Mareels I, et al. Stability and motor adaptation in human arm movements. *Biological Cybernetics* 2005; 94: 22–32.
36. Tee PK, Burdet E, Chew MC and Milner ET. A model of force and impedance in human arm movements. *Biological Cybernetics* 2004; 90: 368–375.
37. Artemiadis PK, Katsiaris PT, Liarokapis MV and Kyriakopoulos KJ. Human arm impedance: Characterization and modeling in 3D space. In: *Proceedings of Intelligent Robots and Systems (IROS)*, 2010, pp. 3103–3108.
38. Masia L and Squeri V. A modular mechatronic device for arm stiffness estimation in human–robot interaction. *Mechatronics, IEEE/ASME Transactions on* 2015; 20: 2053–2066.
39. Wong J, Wilson ET, Malfait N and Gribble PL. The influence of visual perturbations on the neural control of limb stiffness. *Journal of Neurophysiology* 2009; 101: 246–257.
40. Lundstrom R. Local vibrations - mechanical impedance of the human hand's glabrous skin. *Journal of Biomechanics* 1984; 17: 137–144.
41. Yong Jeong H, Gosho T, Higashimori M and Kaneko M. Frequency response dependence to vibration sensitivity by pressing. In: *IEEE International Conference on Robotics and Biomimetics (ROBIO)*, 2009, pp. 1206–1211.
42. Gosselin C, Laliberté T, Mayer-St-Onge B, et al. A friendly beast of burden: a human-assistive robot for handling large payloads. *IEEE Robotics and Automation Magazine* 2013; 20: 139–147.
43. Laliberté T, Gosselin C and Gao D. Closed-loop actuation routings for cartesian scara-type manipulators. In: *Proceedings of the ASME 2010 International Design Engineering Technical Conferences and Computers and Information in Engineering Conference*, 2010, vol. 2, pp. 281–290.
44. Dimeas F and Aspragathos N. Reinforcement learning of variable admittance control for human–robot co-manipulation. In: *Proceedings of the IEEE/RSJ International Conference on Intelligent Robots and Systems (IROS)*, Hamburg, 2015, pp. 1011–1016.
45. Campeau-Lecours A, Foucault S, Laliberte T, Mayer-St-Onge B and Gosselin C. A cable-suspended intelligent crane assist device for the intuitive manipulation of large payloads. *IEEE/ASME Transactions on Mechatronics* 2016. DOI: 10.1109/TMECH.2016.2531626.
46. Campeau-Lecours A, Otis M, Belzile P-L and Gosselin C. A time-domain vibration observer and controller for physical human–robot interaction. *Mechatronics* 2016; 36: 45–53.

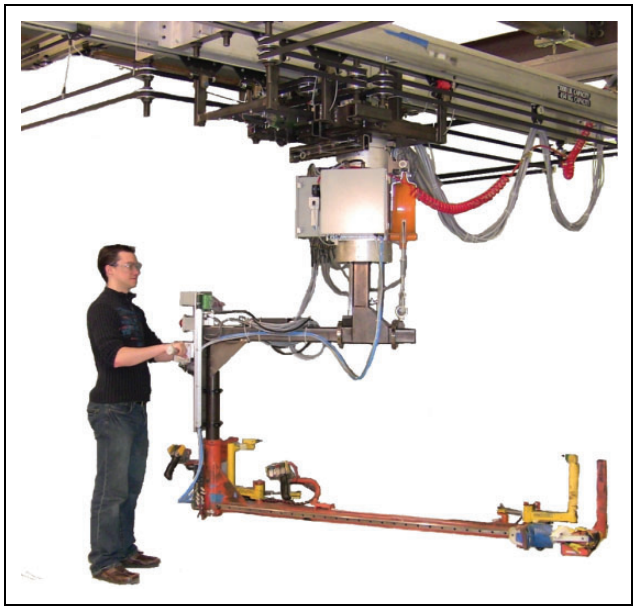

Figure 18. Prototype of a four-degree-of-freedom intelligent assist device.

Appendix I: Prototype of a 4-DOF IAD

The robotic mechanism used for the experiments reported in this paper is the 4-DOF IAD prototype shown in Figure 18, allowing translation in all directions (XYZ) and rotation (θ) about the vertical axis.[42] The total moving mass is approximately 500 kg in the direction of the X axis and 325 kg along the Y axis. The payload may vary between 0 and 113 kg. The horizontal workspace is $3.3\,m \times 2.15\,m$ while the vertical range of motion is 0.52 m. The range of rotation about the vertical axis is 120°. The transmission between the actuators and the end-effector consists of closed-loop toothed belts, as described previously.[43] Three different control modes are possible: autonomous motion, unpowered manual motion and interactive motion (cooperation). In this paper, only the latter is considered. The controller is implemented on a real-time QNX computer with a sampling period of 2 ms (almost five times the IAD bandwidth). The algorithms are programmed using simulink/RT-LAB software (using the following solver options: ode 4, runge-kutta, for the transfer function).

Appendix II: Transfer functions for the improved model

The transfer functions (9) and (11) respectively for the open-loop and closed-loop versions of the elaborate improved model described in the section 'Towards the development of an effective model' are shown below. The transfer function for the open-loop model shown in Figure 9 is written as follows:

$$\frac{V(s)}{F_H(s)} = \frac{K_p(C_B s + K_B)}{(ms + c)(a_4 s^4 + a_3 s^3 + a_2 s^2 + as + a_0)} \tag{9}$$

with

$$\begin{aligned}
a_4 &= (m_R M_R T)\\
a_3 &= (m_R M_R + m_R C_R T + m_R C_B T + C_B M_R T)\\
a_2 &= (K_p M_R + m_R C_B + m_R K_B T + m_R C_R + C_B M_R\\
&\quad + C_B C R T + K_B M_R T)\\
a_1 &= (C_B C_R + K_B M_R + K_B C_R T + K_p C_R + m_R K_B + K_p C_R)\\
a_0 &= (K_p K_B + K_B C_R)
\end{aligned} \tag{10}$$

The transfer function for the closed-loop model shown in Figure 12 is written as follows:

$$\frac{V(s)}{F_H(s)} = \frac{sK_p(C_B s + K_B)(C_H s + K_H)}{\begin{bmatrix} a_6 s^6 + & a_5 s^5 + & a_4 s^4 & \\ + a_3 s^3 + & a_2 s^2 + & a_1 s & + a_0 \end{bmatrix}} \tag{11}$$

with

$$\begin{aligned}
a_6 &= (m m_R M_R T)\\
a_5 &= (m C_B M_R T + m m_R C_R T + m m_R C_B T + m m_R M_R\\
&\quad + c m_R M_R T)\\
a_4 &= (c C_B M_R T + c m_R M_R + m K_p M_R + m m_R C_B\\
&\quad + m m_R C_R + c m_R C_R T + c m_R C_B T\\
&\quad + m K_B M_R T + m C_B C_R T + m C_B M_R + m m_R K_R T)\\
a_3 &= (c C_B C_R T + m m_R K_B + m K_p C_B + m C_B C_R\\
&\quad + m K_B M_R + c C_B M_R + c K_p M_R + c K_B M_R T + c m_R C_B\\
&\quad + m K_p C_R + m K_B C_R T + c m_R K_B T + C_R m_R c)\\
a_2 &= (m K_B C_R + c K_p C_B + m K_p K_B + c K_B C_R T\\
&\quad + K_p C_H C_B + c m_R K_B + c C_B C_R + c K_B M_R + c K_p C_R)\\
a_1 &= (c K_p K_B + K_p K_H C_B + K_p C_H K_B + c K_B C_R)\\
a_0 &= (K_p K_H K_B)
\end{aligned} \tag{12}$$